

Restoring quantum enhancement in realistic two-photon interferometry using spatial information

Michał Jachura, Radosław Chrapkiewicz,* Rafał Demkowicz-Dobrzański, Wojciech Wasilewski, and Konrad Banaszek
Faculty of Physics, University of Warsaw, Pasteura 5, 02-093 Warsaw, Poland

(Dated: December 3, 2024)

Practical realizations of quantum-enhanced interferometry are vulnerable to imperfections such as the residual spectral distinguishability of interfering photons. We demonstrate experimentally that a careful design of the spatial structure of used photons, combined with position-resolved coincidence detection at the output, allows one to recover quantum enhancement for a two-photon Mach-Zehnder interferometer operated in a regime that otherwise cannot even attain the shot-noise limit. This shows the potential of engineering the modal structure of physical systems in metrological applications.

PACS numbers: 42.50.-p, 42.50.Dv, 42.50.St, 42.65.Lm

Quantum mechanics holds the promise to enhance the precision in interferometry and metrology beyond the shot-noise limit [1–10] by preparing collective superposition states of multiple probes (e.g. photons, atoms). Quantum-enhanced measurements exhibit increased vulnerability to imperfections and environmental noise, which can be mitigated by a careful design of the scheme, retaining the benefits of collective preparation [11–17]. In practice, the modal structure of probes, for example photons sent to an interferometer, often becomes an important source of imperfections, which could ultimately preclude beating the standard limits. In the simplest description, such imperfections can be described by a single visibility parameter, which characterizes partial distinguishability of the interfering photons in all degrees of freedom. However, recent advances in single-photon detection offer now unprecedented opportunities to gather detailed information about an individual degree of freedom such as position [18–28]. The purpose of this Letter is to present a proof-of-principle experimental demonstration of how this capability can be used to compensate imperfections in another degree of freedom, for example frequency, thus ensuring quantum-enhanced precision in operating regimes that otherwise cannot even attain the shot-noise limit.

Specifically, we shall consider here the canonical example of a quantum-enhanced phase measurement, when two input ports of a balanced Mach-Zehnder interferometer are each fed with a single photon [29]. The residual spectral distinguishability of interfering photons has a dramatically deleterious effect on the precision of local phase estimation around the operating point when the photons coalesce pairwise at the interferometer output ports. Such a regime can be viewed as a multiphoton generalization of dark-fringe interferometry employed for example in gravitational wave detection [30, 31]. We demonstrate here that by controlling carefully the spatial structure of interfering photons and extracting complete spatial information at the detection stage it is nevertheless possible to achieve sub-shot-noise precision. This

rather surprising result reveals the potential of exploring the complete modal structure of physical systems in metrologic applications.

A generic two-photon Mach-Zehnder interferometer

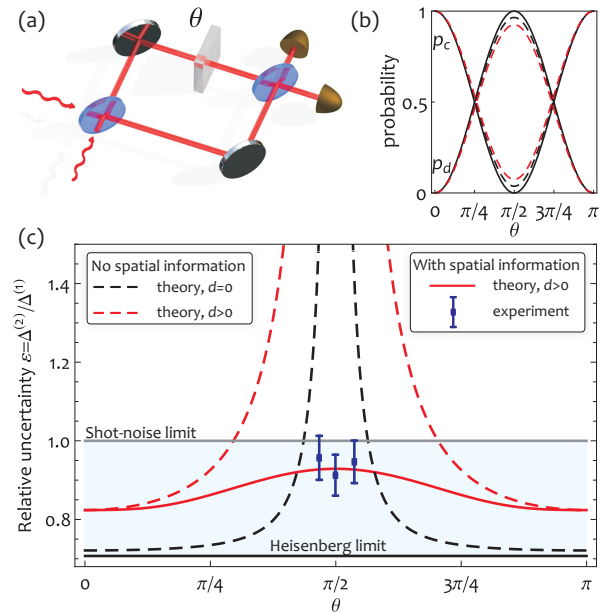


FIG. 1. In a two-photon Mach-Zehnder interferometer (a), the phase shift θ modulates the probabilities of coincidence p_c and double count events p_d at the output (b). The ideal fringes (black solid line) are noticeably affected around $\theta \approx \pi/2$ by imperfect indistinguishability, as depicted for visibilities $\mathcal{V} = 0.93$ (black dashed line) and $\mathcal{V} = 0.85$ (red dashed line). This has a dramatic effect on the uncertainty of phase estimation, shown in (c) with analogously color-coded dashed lines, which diverge at $\theta = \pi/2$ for non-unit visibility \mathcal{V} . Engineering the spatial degree of freedom of the interfering photons and utilizing position information at the output allows one to restore the sub-shot-noise precision, shown with the red solid line calculated for spectral visibility $\mathcal{V} = 0.93$. These predictions are confirmed with experimentally determined estimation precision, depicted as solid squares with two-sigma error bars.

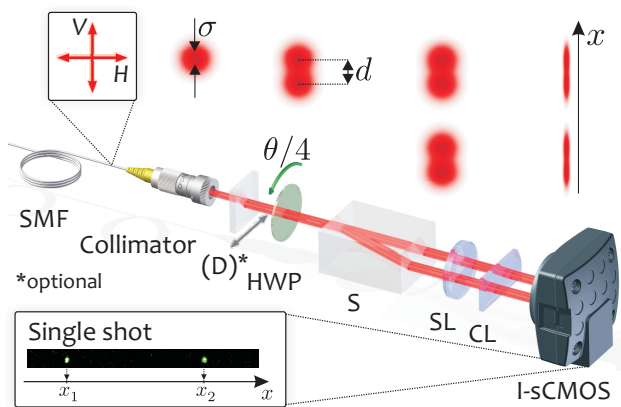


FIG. 2. The experimental setup. Interference between two orthogonally polarized photons delivered by the single mode fiber SMF is realized in the common path configuration with the phase shift θ corresponding to the rotation of the half-wave plate HWP. The output ports of the calcite beam separator S are mapped using a spherical lens SL and a cylindrical lens CL onto the intensified sCMOS camera detecting individual coincidence events with spatial resolution as shown in the inset. An optional calcite displacer D introduces transverse spacing between photon modes, which combined with spatially resolved detection restores the sub-shot-noise precision of the estimated phase shift θ . The upper right part of the figure depicts the spatial profiles of interferometer modes at the consecutive stages with the inserted displacer D.

constructed with a pair of balanced 50/50 beam splitters is shown schematically in Fig. 1(a). The phase shift θ between the interferometer arms modulates probabilities of detection events at the output ports which can be grouped into two types: either the photons exit through different paths, producing a *coincidence event* between the detectors monitoring the ports, or both are found in the same output port leading to a *double event*. If the two photons are indistinguishable at the input, the first beam splitter generates a coherent superposition of both the photons in one or another arm of the interferometer, which is the simplest case of a N00N state providing sensitivity that in the absence of losses approaches the Heisenberg limit [3–5]. In practice, partial distinguishability of interfering photons can be modeled by assuming that a fraction \mathcal{V} of input photon pairs produces the two-photon N00N state, while the remaining $1 - \mathcal{V}$ pairs comprise photons that propagate through the interferometer as independent particles with no multiphoton interference effects. A simple calculation yields the following expression for the probability of a coincidence event

$$p_c(\theta) = 1 - \frac{1}{2}(1 + \mathcal{V}) \sin^2 \theta, \quad (1)$$

while the probability of a double event is $p_d(\theta) = 1 - p_c(\theta)$. The resulting fringes are depicted in Fig. 1(b) for $\mathcal{V} = 1, 0.93$, and 0.85 .

As a consequence of the Cramér-Rao bound [32] the

minimum uncertainty $\Delta^{(2)}$ of any unbiased phase estimate obtained from a measurement using N photon pairs around an operating point θ is given by the inverse of the square root of the Fisher information, which quantifies how much can be inferred about the parameter of interest from all types of available events, and in our case is given by a sum of two terms corresponding to coincidence and double events,

$$\Delta^{(2)} = \left(\frac{N}{p_c(\theta)} \left(\frac{dp_c}{d\theta} \right)^2 + \frac{N}{p_d(\theta)} \left(\frac{dp_d}{d\theta} \right)^2 \right)^{-1/2}. \quad (2)$$

As a reference, we will take the uncertainty of ideal, shot-noise-limited phase measurement $\Delta^{(1)} = 1/\sqrt{2N}$, when $2N$ photons are sent individually to the interferometer. Our figure of merit will be the ratio $\varepsilon = \Delta^{(2)}/\Delta^{(1)}$ of these two uncertainties, with $\varepsilon < 1$ implying that sub-shot noise precision has been achieved.

When the two-photon interferometer is fed with pairs of perfectly indistinguishable photons with $\mathcal{V} = 1$, we have $\varepsilon = 1/\sqrt{2}$ independently of the operating point of the interferometer. It can be verified that around $\theta = 0$ (equivalent to $\theta = \pi$) and $\theta = \pi/2$ the main contribution to Fisher information entering Eq. (2) comes respectively from double or coincidence events that occur with vanishing probabilities when approaching these phase values. This is because in the ideal scenario even a small number of rare events provides a sound basis to infer the phase shift. In the case of standard interferometry such a regime corresponds to dark-fringe operation used e.g. in gravitational wave detectors [30, 31].

As seen in Fig. 1(c), the precision of phase estimation is affected dramatically by the non-ideal indistinguishability of photon pairs. In particular, the precision diverges around $\theta = \pi/2$ owing to the non-vanishing background of coincidence events. Statistical noise generated by this background effectively suppresses information about the phase shift that could be retrieved from coincidence events. An analogous effect would be observed also at $\theta = 0$ if any mechanism generating spurious double events was incorporated in the calculations.

Suppose now that the non-unit value of \mathcal{V} is a result of partial spectral distinguishability of photons within pairs, but we can control the spatial degrees of freedom of the photons and perform position-resolved photodetection. To investigate experimentally this scenario, we constructed an optical setup shown in Fig. 2. The setup is fed with photon pairs generated via type-II parametric process in a 5-mm long periodically poled KTP crystal pumped with 8 mW of 400 nm light from a continuous wave diode laser. The produced pairs are transmitted through a 3 nm FWHM interference filter, carefully synchronized in time using a delay line, and spatially filtered through a single-mode fibre that delivers them to the setup in two mutually orthogonal linear polarizations. These polarizations correspond to the two input ports

of the Mach-Zehnder interferometer. The Gaussian-like spatial modes of the photons have a flat phase and the half-width $\sigma = 122 \mu\text{m}$ at $1/e$ height for the intensity distribution.

To ensure temporal stability, the interferometer transformation is implemented in the common-path configuration as a half-wave plate HWP, with the rotation angle equal to quadruple the phase shift θ between the interferometer arms, followed by a 30 mm long calcite separator S. We determined the residual spectral distinguishability of the photons to yield $\mathcal{V} = 93\%$ by measuring with avalanche photodiodes the depth of the Hong-Ou-Mandel dip for $\theta = \pi/2$. Note that this value has been used in one of the examples presented in Fig. 1(b). After the separator, the transverse distance between the two orthogonally polarized modes corresponding to the output ports of the interferometer is 3.2 mm. The rear surface of the separator S is imaged by means of a spherical lens SL onto a single-photon-sensitive camera system capable of detecting two-photon events with spatial resolution.

The first stage of the camera system is an image intensifier where each detected photon produces a macroscopic charge avalanche resulting in a bright flash at the output phosphor screen [27, 28]. The flashes are subsequently imaged with a high numerical aperture relay lens onto a fast, low-noise $6.5 \mu\text{m} \times 6.5 \mu\text{m}$ pixel (px) size sCMOS sensor and recorded as approx. 25-px wide spots which can be easily discriminated from the low-noise background. The central positions of the spots are retrieved from each captured frame with a subpixel resolution by a real-time software algorithm which provides full information about transverse coordinates of each registered coincidence event as illustrated in the inset of Fig. 2. For the sake of simplicity we consider only the coordinate x in the horizontal plane of the setup and integrate the signals in the vertical direction. The positions of the photons at the calcite surface are mapped onto the sCMOS sensor with a magnification $M = 1.25$ in the horizontal direction. A cylindrical lens CL with $f = 30$ mm in front of the detector was used to reduce the vertical size of the image, producing effectively a $700 \text{ px} \times 22 \text{ px}$ stripe, which significantly decreases frame readout time and allow us to reach 7 kHz collection rate of frames with exposure time 30 ns each. Both the intensifier and the camera are triggered and synchronized by an external digital delay generator.

We recorded spatially resolved two-photon detection events for three values of the phase shift deviating from the $\pi/2$ reference value by $\Delta\theta = \theta - \pi/2 = -0.1, 0, 0.1$, registering approximately 6×10^3 two-photon detection events in each case. Experimentally observed spatial distributions $p_c(x_1, x_2|\theta)$ of two-photon coincidence events, when the photons leave through different output ports of the interferometer, are presented in Fig. 3(a). Qualitatively viewed, these distributions contain virtually no information about the phase shift, in particular there is

no basis to read out the sign of $\Delta\theta$.

In the second series of measurements, we partially separated photons emerging from the fiber by inserting a 1.9 mm long calcite displacer D before the HWP, which results in the displacement of $d = 200 \mu\text{m}$ between the two orthogonally polarized photon modes. The profiles of spatial modes propagating in this case through consecutive stages of the setup are shown in the upper right part of Fig. 2. Fig. 3(b) depicts spatial distributions of coincidence events obtained for displaced input modes. It is seen that the displacement of the input modes clearly restores sensitivity to the phase shift $\Delta\theta$, in particular its sign can be unambiguously inferred from the asymmetry of the distribution. This leads to the question how precisely the phase shift can be estimated from such spatially resolved data.

We will analyze quantitatively the amount of phase information contained in the marginal distribution $p_c(\xi|\theta) = \int dx p_c(x + \xi, x|\theta)$ of the relative position

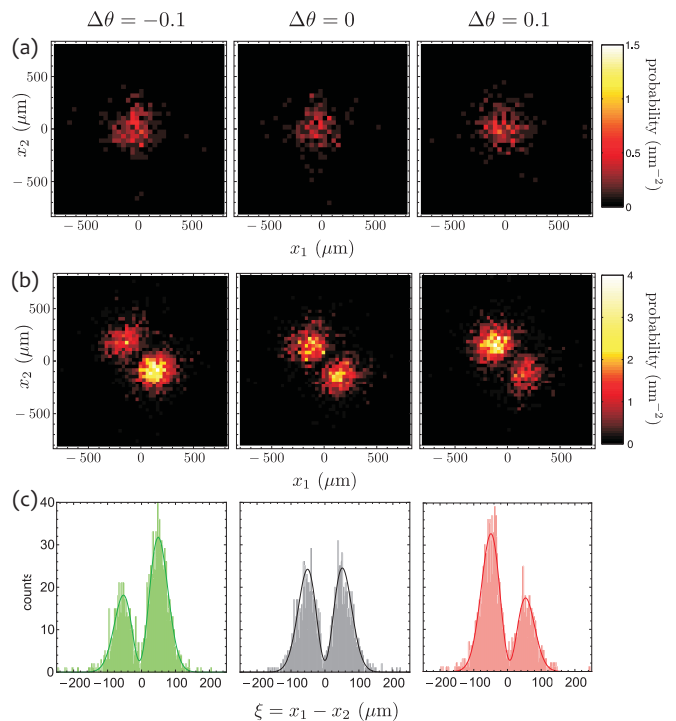


FIG. 3. The joint probability $p_c(x_1, x_2|\theta)$ of detecting two photons at positions x_1 and x_2 in two different output ports of the interferometer for photon pairs characterized by spectral indistinguishability $\mathcal{V} = 0.93$ and prepared in (a) spatially overlapping modes at the input and (b) partially separated spatial modes for three phase shifts $\Delta\theta = \theta - \pi/2$. Although in (b) the spatial mode separation further reduces the photon indistinguishability, the resulting spatial distribution becomes visibly sensitive to the phase shift. Useful information about the phase shift can be extracted from the marginal distributions $p_c(\xi|\theta)$ of the relative position between the photons $\xi = x_1 - x_2$, shown in (c) along with the fits of the theoretical model used in the estimation procedure (solid lines).

$\xi = x_1 - x_2$ between the two detected photons. The corresponding experimental histograms shown in Fig. 3(c) clearly illustrate sensitivity to the phase shift. Assuming Gaussian mode profiles, it is easy to obtain an explicit expression for the marginal distribution of the form

$$p_c(\xi|\theta) = \frac{1}{8\sigma\sqrt{\pi}} \left((1 + \cos\theta)^2 e^{-(\xi-d)^2/4\sigma^2} + (1 - \cos\theta)^2 e^{-(\xi+d)^2/4\sigma^2} - 2\mathcal{V}\sin^2\theta e^{-(\xi^2+d^2)/4\sigma^2} \right). \quad (3)$$

Without position-resolved detection, one would need to integrate $p_c(\xi|\theta)$ over ξ , which yields an expression identical to Eq. (1) with \mathcal{V} replaced by an even lower value $\mathcal{V}e^{-d^2/4\sigma^2}$, where the exponential factor is contributed by spatial distinguishability. In contrast, if the relative position of the photons in coincidence events can be measured, the Fisher information used in Eq. (2) becomes enhanced by replacing the first term in the sum with the following integral over ξ :

$$\frac{1}{p_c(\theta)} \left(\frac{dp_c}{d\theta} \right)^2 \rightarrow F_c(\theta) = \int d\xi \frac{1}{p_c(\xi|\theta)} \left(\frac{\partial p_c(\xi|\theta)}{\partial \theta} \right)^2. \quad (4)$$

For $\mathcal{V} = 0.93$ corresponding to actual spectral distinguishability of photons used in the experiment, minimization of the resulting expression for $\Delta^{(2)}$ at $\theta = \pi/2$ over the displacement yields its optimal value $d = 1.63\sigma$. In Fig. 1(c) we depict the ratio $\varepsilon = \Delta^{(2)}/\Delta^{(1)}$ calculated for these parameters. Strikingly, not only the singular behaviour around $\theta = \pi/2$ is removed, but precision of phase estimation in that region is improved below the shot noise level. This surprising result demonstrates that in certain scenarios effects of residual distinguishability in one degree of freedom, e.g. frequency, can be mitigated by *introducing* carefully engineered excess distinguishability in another degree of freedom, such as position, provided that it can be measured with sufficient resolution at the detection stage.

To confirm the above predictions, we performed phase estimation from the actual experimental data and determined the estimation precision. In the preliminary step, we verified the applicability of Eq. (3) as a statistical model for the collected data assuming independently measured mode parameters $\sigma = 122 \mu\text{m}$ and $d = 200 \mu\text{m}$. We used the maximum-likelihood method to fit \mathcal{V} and θ , obtaining for the three cases depicted in Fig. 3(c) respective phase values $\theta = 1.47(2), 1.57(2), 1.69(2)$ and $\mathcal{V} = 0.93$ which is in agreement with the visibility inferred from the independently measured Hong-Ou-Mandel dip.

In order to determine the actual estimation precision, we divided data obtained for a given HWP setting into approx. 600 subsets of 10 two-photon detection events and estimated the value of the phase shift separately from each subset. Then, the width of the distribution of individual estimates can be used as a figure for the estimation

precision. The choice of the right estimation procedure needs some attention for small sizes of data sets. The maximum likelihood estimator is known to be asymptotically efficient [32] i.e. it saturates the Cramér-Rao bound in the asymptotic limit of infinitely many independent data samples. However, its application to small data sets is not justified owing to its potential biasedness. Therefore we used an estimator which is manifestly unbiased for any data size and yields the precision given by Eq. (2) at least in the vicinity of a given operation point. Specifically, for an experimentally measured statistical frequency distribution $f(\xi)$ of the relative distance between the two photons, this estimator in the vicinity of θ_0 is explicitly given by [10]

$$\tilde{\theta}[f] = \theta_0 + \frac{1}{F_c(\theta_0)} \int d\xi \frac{f(\xi)}{p_c(\xi|\theta_0)} \frac{dp_c(\xi|\theta)}{d\theta} \Big|_{\theta=\theta_0}, \quad (5)$$

where $F_c(\theta)$ has been defined in Eq. (4). The above formula was specialized to $\theta_0 = \pi/2$ with the integral discretized according to the width of the histogram bins. Applying this estimator to individual data subsets yielded a distribution of phase estimates. The estimation precision was determined as the standard deviation of this distribution, shown in Fig. 1(c) for the three phase shifts along with two-sigma error bars. The obtained values, clearly situated below the shot-noise limit, demonstrate quantum enhanced operation of the interferometer despite partial spectral distinguishability of the input photons.

Concluding, the applicability of quantum-enhanced interferometric techniques in practical scenarios crucially depends on the ability to reduce decoherence effects caused by noise and experimental imperfections. Results presented in this paper suggest another class of resources that may help to achieve this regime. Besides obvious attempts to suppress decoherence effects by improving transmission of optical elements, stabilizing phase reference, etc., it proves useful to exploit additional, seemingly independent degrees of freedom of the physical system used for sensing. If the probes are carefully engineered at the input and detected with sufficient resolution at the detection stage, such a strategy can offer a noticeable improvement in precision even though decoherence effects remain at the same level. More generally, this points to the possibility of improving the performance of quantum-enhanced protocols by utilizing routinely ignored degrees of freedom of the physical systems and going beyond the “few-modes”, “few-qubits” paradigms.

Acknowledgments. This project was financed by the National Science Centre No. DEC-2013/09/N/ST2/02229 and by the European Commission under the FP7 IP project SIQS (Grant agreement no. 600645) co-financed by the Polish Ministry of Science and Higher Education.

* radekch@fuw.edu.pl

- [1] C. M. Caves, *Phys. Rev. D* **23**, 1693 (1981).
- [2] B. Yurke, S. L. McCall, and J. R. Klauder, *Phys. Rev. A* **33**, 4033 (1986).
- [3] J. J. Bollinger, W. M. Itano, D. J. Wineland, and D. J. Heinzen, *Phys. Rev. A* **54**, R4649 (1996).
- [4] A. N. Boto, P. Kok, D. S. Abrams, S. L. Braunstein, C. P. Williams, and J. P. Dowling, *Phys. Rev. Lett.* **85**, 2733 (2000).
- [5] V. Giovannetti, S. Lloyd, and L. Maccone, *Phys. Rev. Lett.* **96**, 10401 (2006).
- [6] M. G. A. Paris, *Int. J. Quantum Inf.* **7**, 125 (2009).
- [7] K. Banaszek, R. Demkowicz-Dobrzański, and I. A. Walmsley, *Nature Photon.* **3**, 673 (2009).
- [8] L. Maccone and V. Giovannetti, *Nature Phys.* **7**, 376 (2011).
- [9] G. Tóth and I. Apellaniz, *J. Phys. A* **47**, 424006 (2014).
- [10] R. Demkowicz-Dobrzański, M. Jarzyna, and J. Kołodyński, arXiv:1405.7703 (2014).
- [11] S. F. Huelga, C. Macchiavello, T. Pellizzari, A. K. Ekert, M. B. Plenio, and J. I. Cirac, *Phys. Rev. Lett.* **79**, 3865 (1997).
- [12] U. Dorner, R. Demkowicz-Dobrzański, B. J. Smith, J. S. Lundeen, W. Wasilewski, K. Banaszek, and I. A. Walmsley, *Phys. Rev. Lett.* **102**, 40403 (2009).
- [13] S. Knysch, V. N. Smelyanskiy, and G. A. Durkin, *Phys. Rev. A* **83**, 21804 (2011).
- [14] K. Jiang, C. J. Bragnac, Y. Weng, M. B. Kim, H. Lee, and J. P. Dowling, *Phys. Rev. A* **86**, 013826 (2012).
- [15] A. Datta, L. Zhang, N. Thomas-Peter, U. Dorner, B. J. Smith, and I. A. Walmsley, *Phys. Rev. A* **83**, 63836 (2011).
- [16] B. M. Escher, R. L. de Matos Filho, and L. Davidovich, *Nature Phys.* **7**, 406 (2011).
- [17] R. Demkowicz-Dobrzański, M. Guta, and J. Kołodyński, *Nat. Commun.* **3**, 1063 (2012).
- [18] W. Peeters, J. Renema, and M. van Exter, *Phys. Rev. A* **79**, 043817 (2009).
- [19] H. Shin, K. W. C. Chan, H. J. Chang, and R. W. Boyd, *Phys. Rev. Lett.* **107**, 083603 (2011).
- [20] L. A. Rozema, J. D. Bateman, D. H. Mahler, R. Okamoto, A. Feizpour, A. Hayat, and A. M. Steinberg, *Phys. Rev. Lett.* **112**, 223602 (2014).
- [21] A. F. Abouraddy, M. B. Nasr, B. E. A. Saleh, A. V. Sergienko, and M. C. Teich, *Phys. Rev. A* **63**, 63803 (2001).
- [22] G. Brida, M. Genovese, and I. Ruo Berchera, *Nature Photon.* **4**, 227 (2010).
- [23] M. P. Edgar, D. S. Tasca, F. Izdebski, R. E. Warburton, J. Leach, M. Agnew, G. S. Buller, R. W. Boyd, and M. J. Padgett, *Nat. Commun.* **3**, 984 (2012).
- [24] P.-A. Moreau, F. Devaux, and E. Lantz, *Phys. Rev. Lett.* **113**, 160401 (2014).
- [25] G. B. Lemos, V. Borish, G. D. Cole, S. Ramelow, R. Lapkiewicz, and A. Zeilinger, *Nature (London)* **512**, 409 (2014).
- [26] P. A. Morris, R. S. Aspden, J. E. C. Bell, R. W. Boyd, and M. J. Padgett, *Nat. Commun.* **6**, 5913 (2015).
- [27] R. Chrapkiewicz, W. Wasilewski, and K. Banaszek, *Opt. Lett.* **39**, 5090 (2014).
- [28] M. Jachura and R. Chrapkiewicz, *Opt. Lett.* **40**, 1540 (2015).
- [29] J. G. Rarity, P. R. Tapster, E. Jakeman, T. Larchuk, R. A. Campos, and M. C. Teich, *Phys. Rev. Lett.* **65**, 1349 (1990).
- [30] LIGO Collaboration, *Nature Photon.* **7**, 613 (2013).
- [31] R. Demkowicz-Dobrzański, K. Banaszek, and R. Schnabel, *Phys. Rev. A* **88**, 41802 (2013).
- [32] S. M. Kay, *Fundamentals of statistical signal processing: estimation theory* (Pearson Prentice Hall, Upper Saddle River, NJ, 1993).